AIAA 82-4158

Effective Lateral Thermal Conductivity of Square-Cell Cores

David R. Fairbanks*
Charles Stark Draper Laboratory, Inc., Cambridge, Mass.

The effective thermal conductivity of square-cell cores has been formulated for heat flow lateral to the principal axes of the cells. The formulation is based on a thermal model involving linearized radiation and solid conduction only, where the application is for cored mirrors in space-based optical systems. The formulation uses an effective view-factor correlation that allows a radiative conductance to be isolated as a component acting in parallel with a solid conductance. By analysis for both normal and diagonal global heat flow, relative to the cell pattern, sensitivity of effective thermal conductivity to lateral heat-flow orientation was found to be quite negligible.

Nomenclature

A = equivalent heat-flow area of diagonal model
D = center-to-center cell web spacing
E = cell lateral emissivity factor
E_p = cell parallel emissivity factor
F_e = cell lateral effective view factor
F_p = cell parallel view factor
k = cell web thermal conductivity
k_{ed} = effective diagonal thermal conductivity
k_{en} = effective normal thermal conductivity
k_{ep} = effective parallel thermal conductivity
K_{mn} = thermal conductance from m to n
L = equivalent heat-flow length of diagonal model
l = cell depth parallel to principal cell axes
q_I = ideal radiation heat flow
q_k = linear web conduction heat flow
q_r = equivalent radiation heat flow
q_T = total conduction-radiation heat flow
T_m = mean absolute temperature of cell
T_i = web temperature of unknown i
x = equivalent web conduction width (Fig. 4)
δ = web thickness
ϵ = web surface emissivity
ϵ_s = surface emissivity of sheets facing core
σ = Stefan-Boltzmann constant; 5.67×10^{-8} W/m^2-K^4

Introduction

In recent years, important uses have developed for large optical mirrors in space. In these applications, it is desirable to minimize mirror distortion due to temperature variations and mechanical disturbances and also to produce lightweight mirrors to minimize launch-payload weight. To satisfy these objectives, mirrors have typically been made of materials with very low thermal expansion coefficients (such as fused silica) and low thermal conductivity. Both light weight and high mechanical stiffness are achieved by using a cored structure in which a mirror face sheet and back sheet are separated by a square-cell, core-web matrix that effectively forms a thick sandwich panel. The cells are continuous along their principal axes, normal to the face and back sheets.

The mirror core cells are vented so that in space there is negligible gas convection and conduction. Therefore, heat transfer is due to a combination of radiation and solid conduction. Since the thermal conductivity is low, radiation exchange is important. A rigorous thermal analysis of this type of mirror requires modeling of each individual core web, where each web is subdivided into a number of nodes or finite elements. However, the modeling dimensionality and computational costs would be large.

To avoid this complexity, it is convenient to consider the core to be an equivalent homogeneous solid for which effective thermal property values may be assigned. The effective volumetric heat capacity is readily evaluated as the product of the web material density, specific heat, and core solidity. The effective thermal conductivity values are more difficult to evaluate. In general, the effective conductivity parallel to the principal axes of the cells is significantly different from that normal or lateral to the cell principal axes, and both these values are necessary for adequate thermal modeling of mirrors experiencing nonuniformly distributed thermal loadings.

Previous investigations have concentrated on modeling heat transfer in the parallel direction, since this is the predominant application for honeycomb-cored sandwich panels. A significant amount of analytical modeling and thermal testing has been reported.[1-7] A formula developed by Swann and Pittman[3] gives a reasonably accurate representation of heat flow parallel to the cell principal axes. Reference material[8,9] on effective thermal conductivity of cellular-foamed plastics is not applicable because these structures are of dodecahedral cells and have walls with significant radiation transmissivity.

No reference material has been discovered for either analytical modeling or thermal testing of effective lateral thermal conductivity. This paper presents an analytical formulation of effective lateral conductivity and includes an assessment of the sensitivity of conductivity to angular orientation of global heat flow.

Analysis Methodology

The geometry of the square-cell core is defined in Fig. 1, where, for analysis purposes, the length of the cell along its principal axis (normal to the plane of Fig. 1) is considered to be infinite. The crux of the analysis is to determine the combined effects of web-to-web radiation and web conduction on the temperature distributions and heat flows. These effects were evaluated approximately by multinodal modeling for a design example in which each web (b) and (c) was divided into eight nodal regions. The modeling was based on the assumptions of gray-diffuse surfaces and all web surfaces having equal emissivity values. Temperature differences between web centerlines and their surfaces were assumed small relative to temperature differences across cells. Also, temperature differences across cells are assumed small relative to absolute temperatures, with radiation assumed linear. Web thermal conductivity is considered constant and isotropic. Based on the multinodal modeling results, the combined radiation-conduction behavior could be conveniently separated into a linear web-conduction component

Received March 9, 1981; revision received Oct. 26, 1981.

*Technical Staff, Energy Programs Division.

Table 1 Scaled heat-flow inputs for each conductivity value

k, W/m-K	0	0.130	1.30	13.0	130	∞
q_T, W	0.08494	0.08608	0.09203	0.12698	0.44922	∞
q_k, W	0	0.00036	0.00357	0.03573	0.35731	∞
q_r, W	0.08494	0.08572	0.08846	0.09125	0.09191	—
F_e	0.6845	0.6908	0.7128	0.7353	0.7406	0.7412
$\frac{k\delta}{4\sigma T_m^3 (D-\delta)^2}$	0	0.00288	0.02879	0.2879	2.879	∞

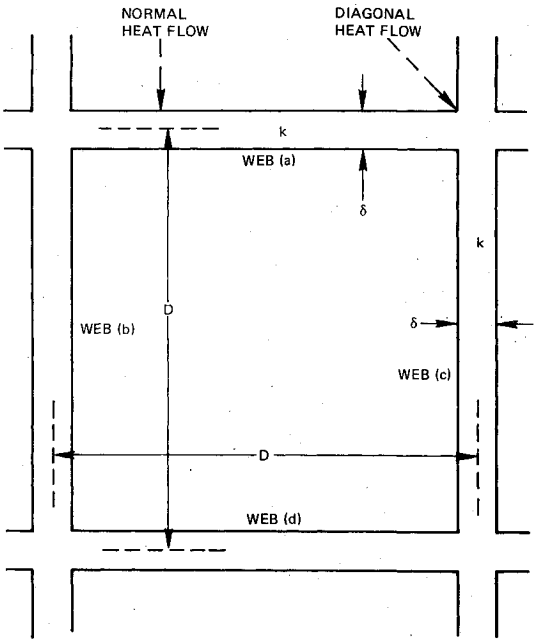

Fig. 1 Square-cell core geometry.

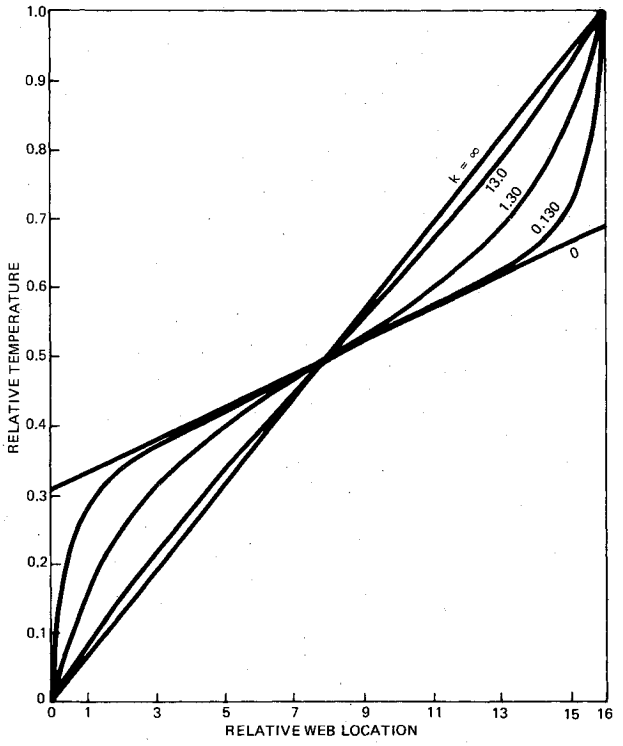

Fig. 2 Wall temperature distributions for webs (b) and (c) vs web thermal conductivity (for the design example).

and a remaining radiation component characterized by an effective view-factor value. These components then could be used in an equivalent conductance network to define an effective conductivity. The most direct analysis is for the case of global heat flow normal to one web surface, which is designated the "normal model." In order to assess sensitivity to angular orientation, an analysis was also performed for global heat flow in the diagonal direction; this is designated the "diagonal model."

Design Example

The design example used as the basis for analysis consists of a fused silica core with a web thermal conductivity k equal to 1.30 W/m-K. The cell spacing D is 12.70 cm, and the web thickness δ is 0.203 cm. Core depth l parallel to the cell principal axes is 54.6 cm. The mean temperature T_m is taken as 295.6 K, for which the linearized radiation coefficient $4\sigma T_m^3$ is 5.86 W/m^2-K. Web surface emissivity values were assumed unity. In order to generalize the results, the multinodal modeling was done with web conductivity k varied over a wide range.

Normal Heat Model

A. Web Temperatures

Figure 1 shows the normal orientation of global heat flow. The radiation incident along web (a) is of unknown distribution, but it is clear that by symmetry (and assumed linear radiation) the net radiation received at any location along the top of web (a) is equal to the net radiation leaving that location along the bottom of web (a). Therefore, since there is no conduction of heat along the web, the midwall temperatures of webs (a) and (d) are each isothermal. For thin webs, the top and bottom surfaces of each web (a) and (d) are nearly isothermal, but are locally affected at the corners by a change in temperature gradient through their thickness due to conduction along webs (b) and (c). For this analysis, the wall surfaces of webs (a) and (d) are each assumed isothermal. The mutually facing wall surfaces of webs (b) and (c) are each divided into eight equally spaced nodal regions for analysis purposes.

Available blackbody radiation view-factor formulas[10] are used, together with view-factor algebra, to determine the nodal radiative couplings. The formula for view factors between nodes on adjacent webs is exact, but the formula for nodes on opposing webs (b) and (c) is for a differential line area on one node. Since the spacing between webs is eight times the node spacing, this expression is reasonably accurate. The inaccuracies involved were adjusted by scaling the view-factor summations along the opposing web so that the total for all three viewed webs is unity. This adjustment amounted to a 5.5% increase. Nodal solid conductance couplings along the webs are included and varied to represent different thermal conductivity values.

This nodal network is solved for an assigned zero sink temperature at web (d) and an arbitrary heat flow input to web (a). The temperature distributions for webs (b) and (c) are then scaled to a unit temperature difference between webs (a) and (d). Solutions were obtained for web thermal conductivity values of 0, 0.130, 1.30, and 13.0 W/m-K. These results are shown in Fig. 2. Also included is a straight line inferred as an asymptotic solution for infinite web thermal conductivity.

B. Effective View Factors

The scaled heat-flow inputs to web (a), associated with each web-conductivity value of Fig. 2, are the combined effects of radiation and conduction. Although these could be directly employed in a formulation for effective conductivity of the core, it is advisable to separate the heat-flow inputs into linear web-conduction components and remaining radiation components. The reasons for this will be apparent in Sec. C. Table 1 shows the scaled heat-flow inputs q_T for each conductivity value. These inputs and the analyses to follow are for a unit depth of core and a unit temperature difference.

The web linear conduction heat-flow values are calculated as

$$q_k = k\delta/(D-\delta) \tag{1}$$

These values are subtracted from the q_T values, and they yield the radiation components q_r. The effective view factors F_e are calculated from

$$F_e = q_r/q_I \tag{2}$$

where $q_I = 4\sigma T_m^3(D-\delta) = 0.1241$ W, which is the idealized amount of heat that would be radiated from web (a), for a unit depth, if all surroundings were at the unit temperature difference. Also included in Table 1 is an extrapolated value, based on Fig. 2, for F_e at $k=\infty$. These F_e values may be correlated with the ratio

$$\frac{q_k}{q_I} = \frac{k\delta}{4\sigma T_m^3 (D-\delta)^2} \tag{3}$$

It is noted that the range of F_e values is only $\pm 4.0\%$ about the mean of 0.7130. It is of interest to compare these F_e values with those for the classical case of adiabatic (disconnected) isothermal reradiating webs (b) and (c), where

$$F_e = 1/\sqrt{2} = 0.7071$$

Although the effects of graybody conditions have not been accounted for in actual web-temperature-distribution modeling, these results may be modified for graybody conditions by use of an emissivity factor E for which F_e may be correlated with the ratio

$$\frac{q_k}{q_I E} = \frac{k\delta}{4\sigma T_m^3 E(D-\delta)^2} \tag{4}$$

The value of E for the case of adiabatic (disconnected) isothermal reradiating webs (b) and (c) is readily found by a radiosity network to be

$$E = \frac{\epsilon}{\epsilon + \sqrt{2}(1-\epsilon)} \tag{5}$$

As an approximation, Eq. (5) may be used to estimate E values for finding F_e. This procedure should be quite accurate for nearly black surfaces, which is the condition existing in the mirror applications of interest. The correlation modified for graybody conditions is plotted in Fig. 3.

C. Equivalent Network

The core equivalent network for defining effective normal core conductivity is composed of two conductances based on q_k and q_r plus the effects of lateral conduction through webs (a) and (d). A local portion of this conduction path effectively acts in series with webs (b) and (c), while the remainder acts in series with the radiation couplings. This situation is depicted in Fig. 4, where the webs are shown separated for clarity. The effective width x of conductance K_{45} must be estimated. For this, the work of Fitzroy[11] indicates that x is equal to 1.38δ.

The conductance

$$K_{45} = kx/\delta = k1.38\delta/\delta \tag{6}$$

may be combined with the conductance

$$K_{56} = k\delta/(D-\delta) \tag{7}$$

to give the equivalent series conductance

$$K_{46} = \frac{1}{(1/K_{45}) + (1/K_{56})} = \frac{k\delta}{D-0.28\delta} \tag{8}$$

The remaining conductances are

$$K_{12} = \frac{k(D-x)}{\delta} = \frac{k(D-1.38\delta)}{\delta} \tag{9}$$

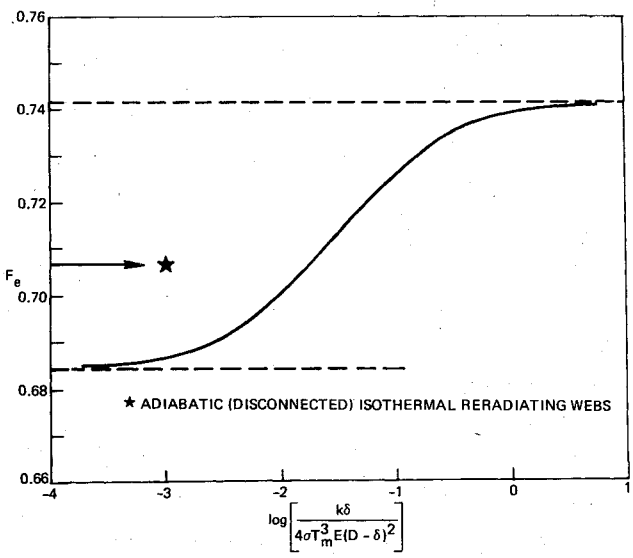

Fig. 3 Relationship between F_e and $\frac{k\delta}{4\sigma T_m^3 E(D-\delta)^2}$.

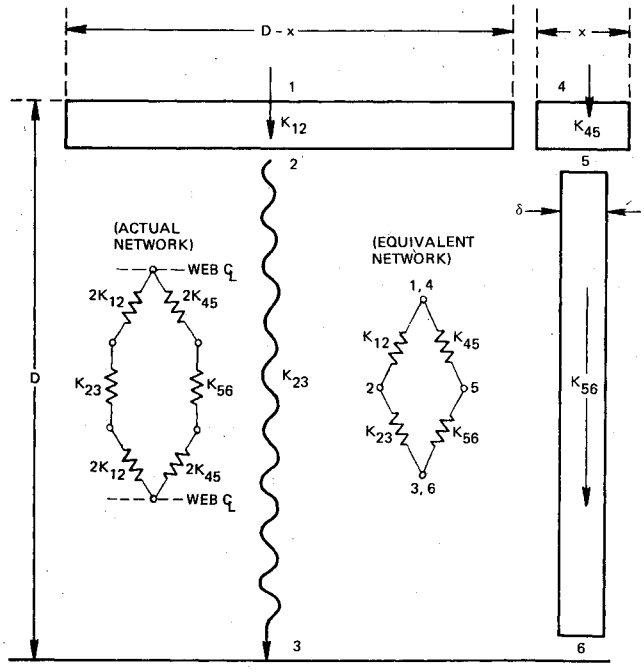

Fig. 4 Normal core equivalent network.

and

$$K_{23}=4\sigma T_m^3 E(D-\delta)F_e \tag{10}$$

D. Effective Normal Conductivity

Because the apparent cross-sectional area and path length for equivalent homogeneous heat flow are equal, the combined overall conductance is equal to the effective thermal conductivity k_{en} so that

$$k_{en}=K_{46}+\frac{1}{1/K_{12}+1/K_{23}} \tag{11}$$

By substituting Eqs. (8-10) into Eq. (11), the effective conductivity of the normal model is

$$k_{en}=\frac{k\delta}{D-0.28\delta}+1\Big/\left[\frac{\delta}{k(D-1.38\delta)}+\frac{1}{4\sigma T_m^3 E(D-\delta)F_e}\right] \tag{12}$$

Diagonal Heat Model

A. Web Temperatures and Effective View Factors

The diagonal direction of global heat flow results in a more implicit blackbody analytical model since all webs experience temperature and heat-flow variations. By symmetry (and assumed linear radiation), however, it is possible to reduce the problem to only a few unknown temperatures. This case may be examined for webs of essentially zero thickness, for which the conduction along the webs is zero but the webs are isothermal through their thickness. The heat balances for the unknown temperatures require examination of two core cells, as indicated in Fig. 5, where a set of temperatures has been assigned to the points of symmetry to represent a global diagonal heat flow. Inspection of this crude network of only two unknowns T_1 and T_2 is enough to disclose the behavior.

First, it is observed that, from the circled node (at temperature $2+T_2$) to symmetrical locations along the adjacent webs (paths a and b), the net heat exchange is identical to that which occurs if both adjacent webs are isothermal at temperature 2. By similar observation, it is evident that the other two (left-hand) adjacent webs are equivalent to being isothermal at temperature 4.

Second, it is observed that, from the circled node to symmetrical locations on the opposing webs (paths c and d), the net heat exchange is identical to that which occurs if each nodal location on the opposing webs is equal in temperature to the corresponding location along the center web containing the circled node.

Such transformed temperatures are identical to those for the normal model with zero-thickness webs. For webs of finite thickness, the temperature distributions would differ, but when the web thickness is small relative to the cell size, this difference would be minor. (See previous discussion.) For purposes of this analysis, the center web temperature distribution (Fig. 5) for the diagonal model is assumed identical to webs (b) and (c) (Fig. 2) for the normal model. Thus, the effective view factors of Table 1 and Fig. 3 apply to the diagonal model.

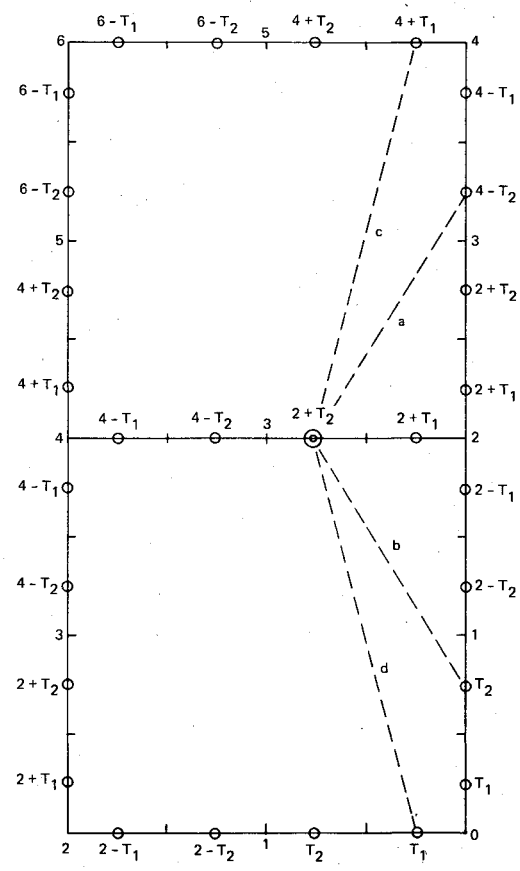

Fig. 5 Diagonal-model radiation conditions.

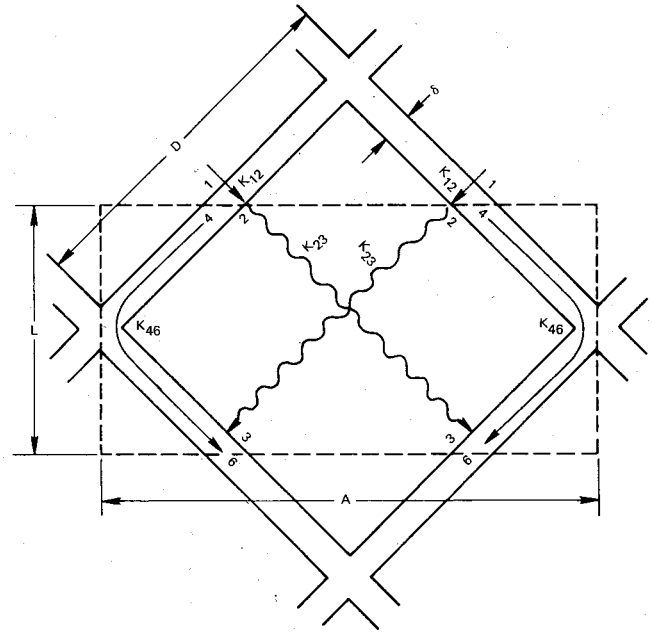

Fig. 6 Diagonal core equivalent network.

B. Equivalent Network and Effective Diagonal Conductivity

In contrast to the core equivalent network for the normal model, the network for the diagonal model is shown in Fig. 6. It is noted that there are two equivalent networks acting in parallel, but these are compensated for by the effective global shape of the model, A/L, which has a value of 2. Although the K_{23} conductance is the same as for the normal model, both K_{12} and K_{46} are slightly altered because they have different conduction geometry at the web-corner intersections.

Because the web conductances K_{12} and K_{46} remain mutually orthogonal at virtually all locations, the width of the K_{12} path is not shortened, so that

$$K_{12}=k(D-\delta)/\delta \tag{13}$$

The K_{46} path is shortened because of the corner turn. A flux plot of the corner is shown in Fig. 7. This indicates an equivalent path of $D/2-0.18\delta$ to the symmetry line at the corner. This makes

$$K_{46}=k\delta/(D-0.36\delta) \tag{14}$$

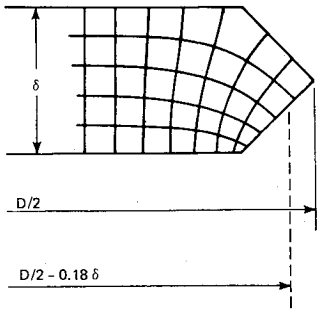

Fig. 7 Web-corner flux plot.

Table 2 Effective conductivity values ($E=1$, $D=12.70$ cm, $T_m=295.6$ K)

δ, cm	k, W/m-K	k_{en}, W/m-K	k_{ed}, W/m-K	$\frac{k_{ed}}{k_{en}}$
0.203	0.130	0.4780	0.4782	1.0004
	1.30	0.5398	0.5399	1.0002
	13.0	0.7470	0.7474	1.0005
	130.0	2.6277	2.6305	1.0011
1.015	0.130	0.3730	0.3761	1.0083
	1.30	0.5911	0.5924	1.0022
	13.0	1.5670	1.5743	1.0047
	130.0	11.125	11.195	1.0063

k, W/m-K	$\frac{k_{en}]_{\delta=1.015}}{k_{en}]_{\delta=0.203}}$
0.130	0.780
1.30	1.095
13.0	2.098
130.0	4.234

The effective thermal conductivity is determined from Eq. (11) with these altered conductance values, so that the effective thermal conductivity of the diagonal model is

$$k_{ed}=\frac{k\delta}{D-0.36\delta}+1\Big/\left[\frac{\delta}{k(D-\delta)}+\frac{1}{4\sigma T_m^3 E(D-\delta)F_e}\right] \quad (15)$$

Discussion

Values of effective conductivity, calculated by using Eqs. (12) and (15) and Fig. 3, are shown in Table 2 for various values of web conductivity and two web thicknesses. It is immediately evident that the normal and diagonal models give almost identical results, particularly for thin webs. The effect of web thickness is very dependent upon web conductivity. At the higher web conductivity values the intuitively expected results occur with increased web thickness; at the lowest conductivity value the reduction in conductance K_{12} dominates, which results in a reduction of effective conductivity with increased thickness. It is interesting to note that, for the design example ($\delta=0.203$ cm, $k=1.30$ W/m-K), the effective conductivity is rather insensitive to changes in web thickness or conductivity. Heat transport is largely controlled by K_{23}, since K_{12} is relatively large and K_{46} is relatively small.

This study did not include the effects of gas within the cells. Gas is negligible in the space applications of interest, and such effects are more complex to analyze, particularly if convection is significant. In the design example, it is estimated[12] that heat transport by air at the surface of the Earth would be dominated by static gas conduction (Rayleigh number of 3000) as long as opposing web temperature differences were less than 0.02 K. In such cases, gas conduction would contribute an additional 6% to the K_{23} term, as an approximation. The influence of gas conduction, relative to radiation, would be increased with smaller cell spacings D.

Effective conductivity in global orientations intermediate to those of the normal and diagonal models is expected to be bounded by the normal and diagonal values. It is thus concluded that, for thin webs, effective conductivity is essentially independent of global heat-flow orientation in the lateral plane.

Effective conductivity in the direction parallel to the core cell principal axes may be estimated by use of an expression[3] reformed into an effective conductivity formula consistent with the assumptions of this study. This formula is

$$k_{ep}=k\left(\frac{2D\delta-\delta^2}{D^2}\right)+4\sigma T_m^3 l F_p E_p \quad (16)$$

where

$$F_p=0.664\left(\frac{\pi l}{4(D-\delta)}+0.30\right)^{-0.69}$$

$$E_p=\epsilon_s^n, \text{ with } n=1.63\left(\frac{\pi l}{4(D-\delta)}+1\right)^{-0.89}$$

In this formula, l is the depth of the core cells between the sheets and parallel to the cell principal axes, and ϵ_s is the common emissivity value of the top and bottom sheets facing the core. F_p and E_p are view-factor and emissivity-factor expressions chosen to fit the data generated by analytical models. The models were accurate representations of circular cells and covered wide ranges of parameter values. The expressions for F_p and E_p fit 1200 analytical k_{ep} values with a maximum deviation of 6.5%. A review of the F_p and E_p expressions discloses that F_p is too large when the cell aspect ratio $\pi l/4(D-\delta)$ is less than unity. It is also noted that the minor functional relationship between F_p and k, which would be expected based on Fig. 3, is omitted. For the design example, Eq. (16) gives a value of $k_{ep}=0.899$ W/m-K. This compares with the value of $k_{en}=0.540$ W/m-K from Table 2. Unfortunately, the tabulated analytical model results[3] for which Eq. (16) was fitted do not extend to the parameter values for the design example.

It is expected that Eqs. (12) and (15) are quite accurate for determining lateral effective conductivity for the case of relatively thin webs, nearly black surfaces, and very long cell depth relative to web spacing. The lateral orientation has been of lesser interest and is more difficult to test because of the need to minimize the cell end effects (at the sandwich sheets) by testing very deep cells. No attempt has been made to find test data for effective lateral conductivity.

In the vicinity of the ends of the cells, the sandwich sheet acts as an additional reradiating wall that effectively reduces the value of F_e locally. It is estimated that this effect is equivalent to a reduction of F_e to about 90% of that determined from Fig. 3 over a distance away from the sheet equal to the web spacing D. In the thermal modeling of a cored mirror using effective conductivity values, these end blockage effects can be accounted for by substituting a reduction of in-plane conductance of the mirror or back-sheet layers adjacent to the core. The mirror and back sheets are modeled separately from the core since they are typically of greater thickness than the webs.

Acknowledgments

This report was prepared by the Charles Stark Draper Laboratory, Inc., and was supported by the Advanced Research Projects Agency of the Department of Defense and monitored by MIRADCOM under Contract DAAK40-79-C-0022.

References

[1]Swann, R. T., "Heat Transfer and Thermal Stresses in Sandwich Panels," NACA TN 4349, Sept. 1958.

[2]Swann, R. T., "Calculated Effective Thermal Conductivities of Honeycomb Sandwich Panels," NASA TN D-171, Dec. 1959.

[3]Swann, R. T. and Pittman, C. M., "Analysis of Effective Thermal Conductivities of Honeycomb-Core and Corrugated-Core Sandwich Panels," NASA TN D-714, April 1961.

[4]Sauer, J. H. Jr. and Nevins, R. G., "Thermal Characteristics of Honeycomb-Core Panels," AIAA Paper 64-257, June 1964.

[5]Kendall, P. J. and Gonzales, J. I., "An Analytical Model for Predicting Thermal Response in Honeycomb Sandwich Panels," AIAA Paper 64-258, June 1964.

[6]Stroud, C. W., "Experimental Verification of an Analytical Determination of Overall Thermal Conductivity of Honeycomb-Core Panels," NASA TN D-2866, March 1965.

[7]Minges, M. L., "Heat Transfer in Structural Honeycomb Composites at High Temperatures," *Proceedings of the Third International Heat Transfer Conference,* Vol. IV, American Institute of Chemical Engineers, 1966, pp. 89-99.

[8]Harding, R. H., "Heat Transfer through Low-Density Cellular Materials," *Industrial and Engineering Chemistry Process Design and Development,* Vol. 3, April 1964, pp. 117-125.

[9]Hammond, M. B. Jr., "An Analytical Model for Determining the Thermal Conductivity of Closed-Cell Foam Insulation," AIAA Paper 68-766, June 1968.

[10]Siegel, R. and Howell, J. R., *Thermal Radiation Heat Transfer,* 2d ed., McGraw-Hill, New York, 1981.

[11]Fitzroy, N. D., *Thermal Conductance of a T or L Shaped Two-Dimensional Configuration,* General Electric DF55GL27, 1955.

[12]Davis, G. de Vahl, "Laminar Natural Convection in an Enclosed Rectangular Cavity," *International Journal of Heat and Mass Transfer,* Vol. 11, Pergamon Press, Great Britain, 1968, pp. 1675-1693.